

Analysis of crack occurs under unsteady pressure and temperature in a natural gas facility by applying FGM

Mohamed A. Eltahir^{*1,2}, Mohamed A. Attia^{2,3}, Ahmed E. Soliman² and Amal E. Alshorbagy²

¹Department of Mechanical Engineering, Faculty of Engineering, King Abdulaziz University, P.O. Box 80204, Jeddah 21589, Saudi Arabia

²Department of Mechanical Design and Production, Faculty of Engineering, Zagazig University, Egypt

³Department of Mechanical Engineering, College of Engineering, Shaqra University, Dawadmi, Saudi Arabia

(Received November 25, 2017, Revised February 11, 2018, Accepted February 12, 2018)

Abstract. Cracking can lead to unexpected sudden failure of normally ductile metals subjected to a tensile stress, especially at elevated temperature. This article is raised to study the application of a composite material instead of the traditional carbon steel material used in the natural gas transmission pipeline because the cracks occurs in the pipeline initiate at its internal surface which is subjected to internal high fluctuated pressure and unsteady temperature according to actual operation conditions. Functionally graded material (FGM) is proposed to benefit from the ceramics durability and its surface hardness against erosion. FGM properties are graded at the radial direction. Finite element method (FEM) is applied and solved by ABAQUS software including FORTRAN subroutines adapted for this case of study. The stress intensity factor (SIF), temperatures and stresses are discussed to obtain the optimum FGM configuration under the actual conditions of pressure and temperature. Thermoelastic analysis of a plane strain model is adopted to study SIF and material response at various crack depths.

Keywords: fracture mechanics; functionally graded pipe; finite element; pressure fluctuation; radial crack; stress intensity factor; thermoelastic analysis

1. Introduction

Natural gas pipeline should meet more demanding requirements than that are used at oil industry because it carries highly compressed multiphase flammable gases at variable temperatures change from 80°C at compression to -25°C at expansion, which makes the crack growth and brittleness a serious problems in these severe operating conditions. At a natural gas facility in Egypt, erosion of the internal surface of a natural gas pipeline happened then it led to a crack resulted in shutdown. Because of this problem an alumina lining of the carbon steel pipes is suggested to resist erosion. The variation of properties between alumina and carbon steel may lead to cracks at the intermediate surface because of the variation of material properties. This leads to the need to study FGMs as a modern alternative to get the alumina advantages of erosion resistance in addition to improve the stress distribution and reduce the stress concentration.

Anderson (2005) mentioned that the stress corrosion cracking (SCC) which is the growth of crack formation in a corrosive environment can lead to unexpected sudden failure of normally ductile metals subjected to a tensile stress; especially at elevated temperature; but, Ceramics attack is significantly less common because ceramics are more resistant to chemical attack. Although phase changes are common in ceramics under stress, these usually result in

toughening resulting in slow crack growth rather than sudden failure of dense ceramic bodies. Prevent SCC initiation is gained by the material selection, the limitation of stress and the control of the environment. Shi *et al.* (2010) developed A three-dimensional extended finite element method (XFEM) coupled with a narrow band fast marching method and implemented in the ABAQUS for curvilinear fatigue crack growth and life prediction analysis of metallic structures. Pan *et al.* (2016) proposed a fracture mechanics model for FGM strip divided into multilayers with general thermomechanical properties and collinear cracks under thermal loading. Using superposition method to reduce the problem to a perturbation problem then to integral equations by generalized Cauchy kernel and solving numerically. Hein and Kuna (2016) presented the derivation of the 3D J-integral implemented in FEM by means of the equivalent domain integral technique for arbitrary location and temperature dependent material presented by a thermally loaded plate of FGM with a surface crack. Eshraghi *et al.* (2016) studied the transient thermo-mechanical SIF for FG cylinders with complete internal circumferential cracks by the weight function method. The finite difference method was used to calculate the time dependent temperature distribution and thermal stresses along the cylinder thickness and the finite element analysis (FEA) was used to determine the weight function coefficients and to investigate the accuracy of the predicted SIF from the weight function.

Rajabi and Soltani (2016) studied Mixed-mode thermal fracture of cracked AISI 304 austenitic stainless-steel layers under thermal gradients of cryogenic and elevated temperatures. The J_k -integral method, incorporating

*Corresponding author, Associate Professor

E-mail: mohaeltaher@gmail.com or meltaher@kau.edu.sa or mmeltaher@zu.edu.eg

temperature-dependent material properties, was used to determine the mixed-mode SIF from the results of FEA. Eskandari (2016) analyzed the 3D fracture of thick walled FGM cylinder, containing a longitudinal semielliptical internal surface flaw, and was subjected to an internal pressure and a rotational speed. The material gradation, the crack geometry and wall thickness had an influence on the SIF. Hamed *et al.* (2016) investigated the fracture behavior of sigmoidal FG nanobeam by using finite element method. Eskandari (2016) analyzed the 3D fracture of a pressurized cylinder with hoop wrapped FGM layer containing a longitudinal semielliptical internal surface crack and subjected to temperature gradient. The hoop wrapped FGM influenced the SIF along the crack front. Nimje and Panigrahi (2016) analyzed the effects of FG adhesive on failures in the socket joints of laminated fiber reinforced polymer (FRP) composite tubes and studied various types of failures in the socket joint using strength of materials and fracture mechanics approach. Fu *et al.* (2016) investigated the thermoelastic problem of a transversely isotropic hollow cylinder containing a circumferential crack based on the non-Fourier heat conduction theory. The temperature and stress fields are obtained by solving the coupled partial differential equations in the Laplace domain, and corresponding the thermal axial stress with minus sign was applied to the crack surface to form a mode I crack problem. Three different kinds of crack were considered, and the singular integral equation method was adopted to solve the fracture problem.

De Schiara *et al.* (2016) exploited Finite element mesh generation for fracture mechanics in 3D coupled with ANSYS to study the elliptical cracks at fusion in the nozzle welds. Burlayenko *et al.* (2016) analyzed numerically the thermal cracking in a ceramic/metal FG plate under thermal shock loading by ABAQUS to find the temperature field and associated thermal stresses. A linear quasi-static thermoelastic problem for plane strain state was solved. The distribution of temperature and thermal induced stresses which are accounting for residual stresses inside the plate were calculated under the conditions of both steady state and transient thermal processes. The solution of the transient heat conduction problem was used for the crack propagation simulation using the virtual crack closure technique. Lei (2016) performed theoretical and numerical validations for the ABAQUS contour integral J and C(t) functions and used a self-developed software for cases with residual stresses followed by cracked-body fracture/creep analyses. Mirsayar and Takabi (2016) studied the tangential strain distribution and fracture initiation conditions for underwater notched structures subjected to hydrostatic pressure using FE simulation of a V-notched semi-circular specimen. It was shown that not only the singular terms, but also the “constants train field” significantly influenced the tangential strain distribution and fracture initiation angle around the notch tip. Sharma *et al.* (2016) carried out XFEM simulation to investigate the fatigue life of a FGM under cyclic mixed mode loading and the effect of presence of minor cracks, holes and inclusions of arbitrary sizes randomly located in the domain along the major crack. Paris law was used to evaluate the fatigue life. Sladek *et al.* (2016) used the quarter-point crack tip element to derive a

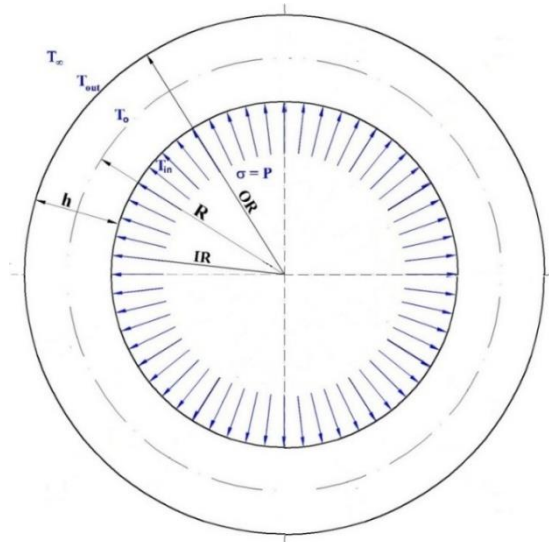


Fig. 1 Geometry and boundary conditions

formula to evaluate the elastic T-stress by FEM at FGMs comparing the variation of displacements in the quarter-point element with the corresponding asymptotic expression for the displacement field in the vicinity of a crack-tip. Francisco *et al.* (2016) studied the effect of pre-crack in the fracture properties of steel pipes used in oil type API-5L-X70. Shariati *et al.* (2017) investigated the variations of mode I stress intensity factor (K_I) for the inner penny-shaped and circumferential cracks in FG hollow thick-walled cylinder consists of epoxy and glass with the changes of crack geometry, material gradation and loading conditions. The equations of motion obtained from XFEM were solved by the Newmark method in the time domain. The interaction integral method was employed to calculate K_I . The MATLAB programming environment was implemented to solve the problem. Rizov (2017) presented a theoretical study of delamination fracture in Crack Lap Shear (CLS) functionally graded beam configuration. The basic purpose was to analyze the fracture by taking into account the non-linearity of material. Nabil *et al.* (2017) modelled a crack propagating through a finite element mesh under mixed mode conditions. Soilman *et al.* (2018) investigated the response of functionally graded (FG) gas pipe under unsteady internal pressure and temperature using finite element method.

In this study the FGM is proposed and the material properties are graded at the radial direction. FEM is applied and solved by ABAQUS software including FORTRAN subroutines adapted for this case of study. SIF, temperatures and stresses are discussed to obtain the optimum FGM configuration under the actual conditions of pressure and temperature. Thermo-mechanical analysis of a plain strain model is adopted to study the SIF and the material response at various crack depths.

2. The mathematical model formulation

2.1 Geometry description

The cross section of a pipe with 112 mm outer diameter

Table 1 Materials properties of the metal (Carbon steel A106Gr.B) and the ceramic (alumina, Al₂O₃)

Properties	Ultimate tensile strength (GPa)	Yield strength (GPa)	Mass density (kg/m ³)	Young's modulus (GPa)	Poisson's ratio	Specific heat (J/kgK)	Thermal Conductivity (W/m.K)	Thermal expansion Coefficient, (/K)
A106Gr.B	0.54	0.415	7870	200	0.29	472	51.9	1.17E-05
Alumina	0.665	0.665	3800	380	0.3	880	10.4	7.40E-06

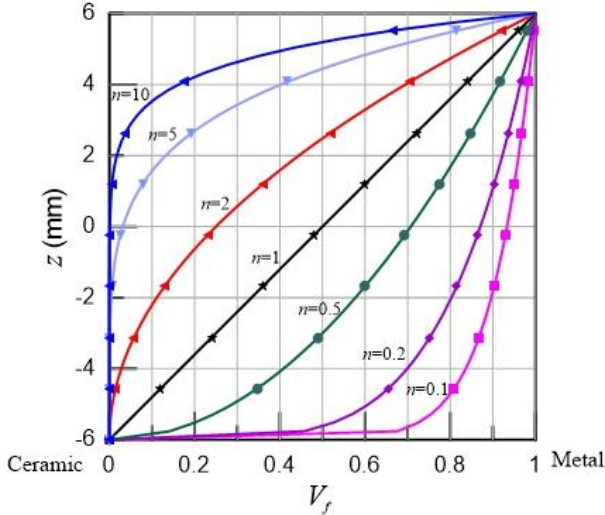


Fig. 2 Volume fraction of P-FGM pipe

similar to that is used in a natural gas facility. The mean radius is $R = 50$ mm, and pipe thickness is $h = 12$ mm, $-\frac{h}{2} \leq z \leq \frac{h}{2}$, (i.e., $-6 \leq z \leq 6$) Fig. 1. The analysis of a radial crack at the inner surface is carried out for cracks of various widths from 1 mm to 11 mm.

2.2 Material characteristics

FGM variation is dictated by a parameter “ n ”. The “ n ” value is of significance because it is the exponent of the volume fraction equation. “ n ” value essentially dictates the amount and distribution of ceramic in the shell. By increasing “ n ” values, the distribution of material tends towards ceramic (the inner surface). While by lowering the “ n ” values, the material tends toward metal (the outer surface). At $n = 0$ the shell is fully metallic while at $n = \infty$ the shell is fully ceramic. Material properties E , G , ρ , α , and k are mentioned as $E(z)$ and are dependent on the n value and the position in the thickness so it varies according to the power law, (Alshorbagy *et al.* (2011, 2013), Eltahir *et al.* (2013a, b))

$$E(z) = E_c + (E_m - E_c)V_f \quad V_f = \left(\frac{z}{h} + \frac{1}{2}\right)^n \quad (1)$$

$z = 0$ denotes the middle of the shell, and $z = \pm h/2$ denotes the outer and inner surfaces of the pipe.

The variations of volume fraction through thickness for $n = 0.1$, $n = 0.2$, $n = 0.5$, $n = 1$, $n = 2$, $n = 5$, and $n = 10$ are compared Fig. 2.

The proposed materials are Carbon steel API.5L-X65 as a metal which has more ductility, better thermal conductivity, lower specific heat and lower stiffness and alumina (Al₂O₃) as ceramic which has corrosion resistance,

better toughness, lower expansion coefficient and lower density. The material properties of these materials are presented in Table 1 (Swaminathan and Sangeetha 2017).

2.3 Governing equation

To analyze the thermoelastic behavior of the pipe, a plane strain problem is assumed to describe the constitutive behavior of the cross section in cylindrical form as

$$\begin{cases} w_{\theta} = \begin{cases} \frac{b_j x_i}{6EI} (l^2 - x_i^2 - b_j^2), & \text{for } i \leq j \\ \frac{b_j}{6EI} \left[\frac{l}{b_j} (x_i - a_j)^3 + (l^2 - b_j^2) x_i - x_i^3 \right], & \text{for } i > j \end{cases} \\ u_i = \frac{x_i}{24EI} (l^3 - 2lx_i^2 + x_i^3) \end{cases} \quad (2)$$

where (σ_r) is the radial stress component, (σ_{θ}) is the hoop stress component, $(\sigma_{r\theta})$ is the shear stress component, (ε_r) is the strain component at the radial direction, (ε_{θ}) is the strain component at the hoop direction, $(2\varepsilon_{r\theta})$ is the shear strain component, (E) is the modulus of elasticity, (ν) is the Poisson's ratio.

The infinitesimal strains-displacement relationships are given as

$$\left. \begin{aligned} \varepsilon_r &= \frac{\partial u_r}{\partial r} \\ \varepsilon_{\theta} &= \frac{u_r}{r} + \frac{1}{r} \frac{\partial u_{\theta}}{\partial \theta} \\ 2\varepsilon_{r\theta} &= \frac{1}{r} \frac{\partial u_r}{\partial \theta} + \frac{\partial u_{\theta}}{\partial r} - \frac{u_{\theta}}{r} \end{aligned} \right\} \quad (3)$$

where (u_r) is the component of displacement at the radial direction, (u_{θ}) is the component of displacement at the hoop direction, (θ) is the angle, (r) is the radius.

2.4 The equilibrium equation (equation of motion)

The equilibrium equation of linear elastic fracture in a hollow cylinder, disregarding the body forces is

$$\left. \begin{aligned} \frac{\partial \sigma_r}{\partial r} + \frac{1}{r} \frac{\partial \tau_{r\theta}}{\partial \theta} + \frac{\sigma_r - \sigma_{\theta}}{r} &= 0 \\ \frac{1}{r} \frac{\partial \sigma_{\theta}}{\partial \theta} + \frac{\partial \tau_{r\theta}}{\partial r} + \frac{2\tau_{r\theta}}{r} &= 0 \end{aligned} \right\} \quad (4)$$

2.5 Heat transfer equations

The transient heat conduction is determined by

$$\frac{1}{r} \frac{\partial}{\partial r} \left(rk(r) \frac{\partial T(r,t)}{\partial r} \right) + \frac{1}{r^2} \frac{\partial}{\partial \theta} \left(k(r) \frac{\partial T(r,t)}{\partial \theta} \right) = \rho(r)C(r) \frac{\partial T(r,t)}{\partial t} \quad (5)$$

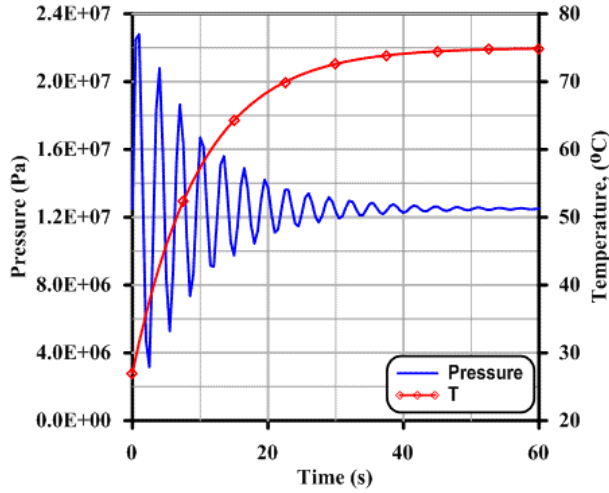


Fig. 3 Pressure and temperature variation

where $k(z)$, $\rho(z)$, and $c(z)$ are the thermal conductivity, the mass density, and the heat capacity, respectively.

2.6 Dynamic pressure load

The dynamic pressure of the natural gas in the pipeline is studied according to a proposed formula because of its irregular behavior

$$P = P_o \times \left(1 + \frac{\sin(2 \times t)}{e^{\left(\frac{t}{10}\right)}} \right) \quad (6)$$

where, P is the gas pressure inside the pipe and P_o is the steady state pressure, $P_o = 1.2$ MPa Fig. 3.

2.7 Thermal load

The change of the internal temperature is assumed at the inner surface according to the exponential equation.

$$T_s = T_n - (T_n - T_o) \cdot e^{-\gamma t} \quad (7)$$

where T_s is the inner surface temperature, T_o and T_n are the inner surface initial and eventual temperatures respectively, $T_o = 27^\circ\text{C}$ and $T_n = 7^\circ\text{C}$. γ is the coefficient of temperature change rate, $\gamma = 0.1$, and t is the time in seconds Fig. 3.

2.8 Boundary conditions

$$u_\theta(r, 0) = u_\theta\left(r, \frac{\pi}{2}\right) = 0 \quad (8)$$

The thermal boundary conditions include the pipe initial temperature $T_o = 27^\circ\text{C}$, T_∞ denotes the atmospheric temperature $T_\infty = 27^\circ\text{C}$ and h_o is the convection coefficient, $h_o = 50$ W/m²C.

$$k(z) \frac{\partial T(r_o)}{\partial r} + h_o(T - T_\infty) = 0 \quad (9)$$

$$T_s(r, \theta, 0) = T_o \quad (10)$$

2.9 Fracture analysis

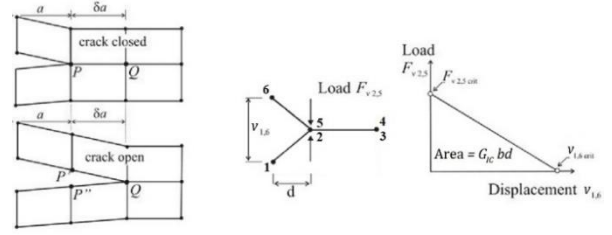


Fig. 4 Mode I crack open and closure and crack growth criterion

Stress intensity factor (K_I)

The stress intensity factor (SIF) for the edge crack of opening mode-I can be calculated from the strain energy release rate (SERR) G_I .

$$-\frac{1}{2} \frac{F^Q \Delta U^P}{\Delta A} = G_I \quad (11)$$

where $\Delta A = \delta a b$ is the area of crack surface of width b formed due to the crack extension δa . F^Q and ΔU^P are the reaction force at node Fig. 4.

$$K_I^2 = G_I \left(\frac{E}{1 - \nu^2} \right)_{tip} \quad (12)$$

The modulus of elasticity (E) and the Poisson's ratio (ν) are gained at the crack tip.

$$-\frac{1}{2} \frac{F_{v2,5} v_{1,6}}{b d} = G_I \geq G_{IC} \quad (13)$$

where G_{IC} is the mode I critical SERR related to the critical SIF, i.e., fracturing toughness. $F_{v2,5}$ is the reaction force between node 2 and 5. $v_{1,6}$ is the OD between nodes a and 6. b is the width and d is the length of the element at crack front Fig. 4, Burlayenko (2016).

Stress Fields ahead of a crack tip

For mode I in a linear elastic isotropic plane strain material, Anderson (2005)

$$\left. \begin{aligned} \sigma_{rr} &= \frac{K_I}{4\sqrt{2\pi r}} \left[5 \cos\left(\frac{\theta}{2}\right) - \cos\left(\frac{3\theta}{2}\right) \right] \\ \sigma_{\theta\theta} &= \frac{K_I}{4\sqrt{2\pi r}} \left[3 \cos\left(\frac{\theta}{2}\right) + \cos\left(\frac{3\theta}{2}\right) \right] \\ \tau_{r\theta} &= \frac{K_I}{4\sqrt{2\pi r}} \left[\sin\left(\frac{\theta}{2}\right) + \sin\left(\frac{3\theta}{2}\right) \right] \\ \sigma_{zz} &= \nu(z)(\sigma_{rr} + \sigma_{\theta\theta}) \end{aligned} \right\} \quad (14)$$

3. Numerical formulation

3.1 The finite element formulation

The displacements of nine-node iso-parametric quadrilateral finite element are

$$\{u\} = [N_N] \{u^N\} \quad (15)$$

as N_N are the interpolation functions which depend on the coordinate system of material, u^N is the nodal

displacement vector. After applying the interpolation shape functions, strains are obtained from displacements by differentiation as

$$\{\varepsilon\} = [B]\{u\} \quad (16)$$

where B is the shape functions derivatives strain-displacement matrix, so the stress-strain relation is

$$\{\sigma\} = [D](\{\varepsilon\} - \{\varepsilon_0\}) \quad (17)$$

where D is the constitutive matrix and ε_0 is the initial strain (thermal strain). By applying the virtual work principle the finite element stiffness equation is

$$[K]\{u\} = \{F\} \quad (18)$$

where F is the load vector and the finite element stiffness matrix (K) is

$$[K] = t_e \int_{-1}^1 \int_{-1}^1 [B]^T [D] [B] [detJ] d\xi d\eta \quad (19)$$

where ξ and η are the natural coordinates.

The stresses in the quadrilateral element are not constant within the element; the stresses are evaluated at the Gauss points. Quadrilateral shape has a better convergence rate and is less affected by mesh orientation than triangles.

The quadratic interpolation for 9 nodes iso-parametric element is

$$T^e(r, \theta, t) = [N_i(r, \theta)]\{q_i(t)\}^e, \quad i = 1, 2, \dots, 9 \quad (20)$$

3.2 The coupled thermo-elastic analysis

Coupled thermo-elasticity equations are used to find the solution for the stress-displacement and temperature fields simultaneously when the thermal and mechanical solutions affected greatly by each other. It is mainly valid for small temperature changes, but it has been used for relatively high temperature changes as well. Backward-difference method is used to integrate the temperature heat transfer equation, and Newton's method is used in solving the nonlinear coupled system. Coupled equations non-symmetric Jacobian matrix is

$$\begin{bmatrix} K_{uu} & K_{u\theta} \\ K_{\theta u} & K_{\theta\theta} \end{bmatrix} \begin{Bmatrix} \Delta u \\ \Delta \theta \end{Bmatrix} = \begin{Bmatrix} R_u \\ R_\theta \end{Bmatrix} \quad (21)$$

where Δu , $\Delta \theta$ are particular corrections of the incremental displacement and temperature, K_{ij} is a sub-matrices of the fully coupled Jacobian matrix and R_u, R_θ are the mechanical and thermal residual vectors. When the coupling between the two solutions is weak the off-diagonal sub-matrices are neglected.

$$\begin{bmatrix} K_{uu} & 0 \\ 0 & K_{\theta\theta} \end{bmatrix} \begin{Bmatrix} \Delta u \\ \Delta \theta \end{Bmatrix} = \begin{Bmatrix} R_u \\ R_\theta \end{Bmatrix} \quad (22)$$

The minimum usable time increment and the element size in transient analysis with second-order elements is

$$\Delta t > \frac{\rho c}{6k} \Delta l^2 \quad (23)$$

where Δt is the time increment, ρ is the mass density, c is the specific heat, k is the thermal conductivity and Δl is the

element dimension (length of its side).

3.3 Numerical integration method

For dynamic Analysis, the load vector has the form

$$F^N = -M^{NM}\ddot{u}_{t+\Delta t}^M + (1 + \alpha)G_{t+\Delta t}^N - \alpha G_t^N \quad (24)$$

where M^{NM} is the element mass matrix, G^N is the static load vector and α is the Hughes-Hilbert-Taylor (HHT) integration operator.

The Jacobian has the form

$$M^{NM} \left(\frac{d\ddot{u}}{du} \right) + (1 + \alpha)C^{NM} \left(\frac{d\dot{u}}{du} \right) + (1 + \alpha)K^{NM} \quad (25)$$

where, C^{NM} is the element damping matrix and K^{NM} is the static tangent stiffness matrix.

$$\frac{d\ddot{u}}{du} = \frac{1}{\beta\Delta t^2} \quad \text{and} \quad \frac{d\dot{u}}{du} = \frac{\gamma}{\beta\Delta t} \quad (26)$$

where, $\beta = \frac{(1-\alpha)^2}{4}$ and $\gamma = \frac{1}{2} - \alpha$ are the coefficients in the Newmark- β operator.

The weak form provides the integration

$$\int_{\Omega} \left[k(z) \left(\frac{\partial T(r, \theta, t)}{\partial r} \right)^2 + \frac{k(z)}{r^2} \left(\frac{\partial T(r, \theta, t)}{\partial \theta} \right)^2 + 2\rho(z)c(z) \left(\frac{\partial T}{\partial t} \right) \right] d\Omega = 0 \quad (27)$$

The pipe is described by 2-D plane strain problem. The finite element model is created using the finite element analysis software ABAQUS. The thermal and mechanical properties are imbedded into the model by the definition of each property at the Gauss points of the finite element through the ABAQUS user-defined subroutines. The user defined field (USDFLD) is used to apply the mechanical and thermal properties; while the user amplitude (UAMP) is used to apply the thermal and mechanical loads. The solution consists of thermo-mechanical analysis, stress analysis and failure analysis. In the thermo-mechanical analysis, the pipe is assumed to be internally pressurized according to Eq. (6) and its internal surface temperature is according to Eq. (7) with free convection at the outer surface.

A fully coupled thermal-stress analysis in ABAQUS/Standard is employed to evaluate the distributions of transient temperature and stresses. The computed transient stress fields which are known at each point of the model as a function of temperature and material gradient are used as driving forces for the crack growth in the pipe. The 2-D model is discretized by quadratic plane strain elements (CPE8T) for thermal and displacement analyses. The crack is modeled by an actual small gap between the finite elements located along the crack surfaces. In the fracture analysis, to simulate the stress singularity in the vicinity of the crack tip and to extract the SIF, the degenerated quarter-point quadratic elements are used and these singular crack-tip elements are surrounded by the standard nine-node quadratic elements for the rest of the two-dimensional model. The radius of these elements is

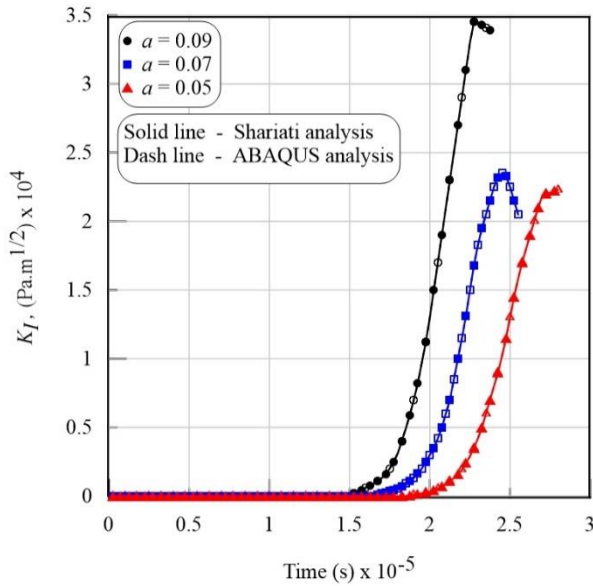


Fig. 5 SIF for crack embedded in a FG cylinder under impulsive tension

taken as $0.05a$ to compute the SIF. The contour integral in terms of the energy release rate and, hence, the stress intensity factor is calculated by utilizing the domain integral.

4. Results and discussion

4.1 The validation of the method

The model applied here is validated with the results obtained by Shariati (2017) for FG cylinder with material gradient according to a power law and parameter $P = 0.2$ and is subjected to a uniform impulse tensile stress $\sigma = 1$ MPa at time $t = 1\mu\text{s}$ applied to the upper surface of the cylinder. The curves of SIF for different crack radius (a) are plotted in Fig. 5. As shown, It is noted that, the obtained results are identical agreement with that obtained by Shariati (2017).

4.2 Numerical results

To evaluate the best material configuration for the pipeline, three configurations of the pipe materials are applied. the first pipe is composed of 8 mm carbon steel (API-5L-X65) which is lined with 4 mm Alumina from inside, the second pipe is composed of 8 mm of carbon steel (API-5L-X65) which is lined with 4 mm FGM from inside and the third pipe material is FGM with 12 mm thick. The temperature variation depends on the material composition of the pipe because the Alumina has lower conductivity than carbon steel and this is obvious in the variation of the temperature at different depths and times as shown in Figs. 6 and 7. The variation of temperature depends on the distribution of ceramic by the power factor of the FGM. So, at 1 mm depth from inside, the ceramic component has more influence on the heat transferred toward outside.

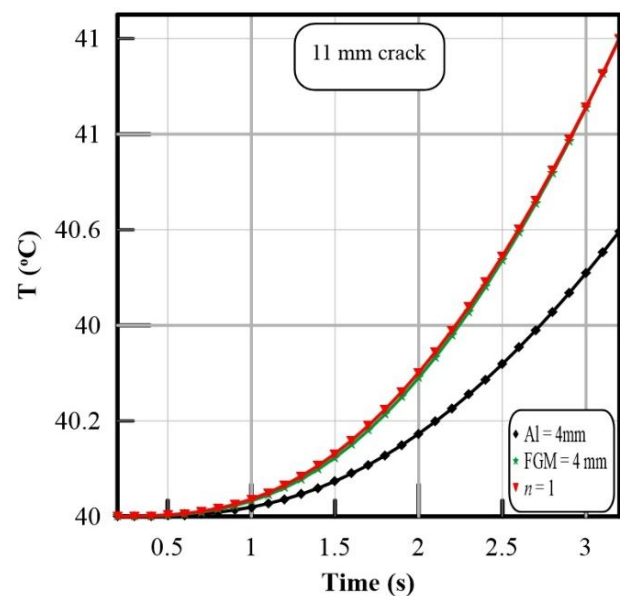
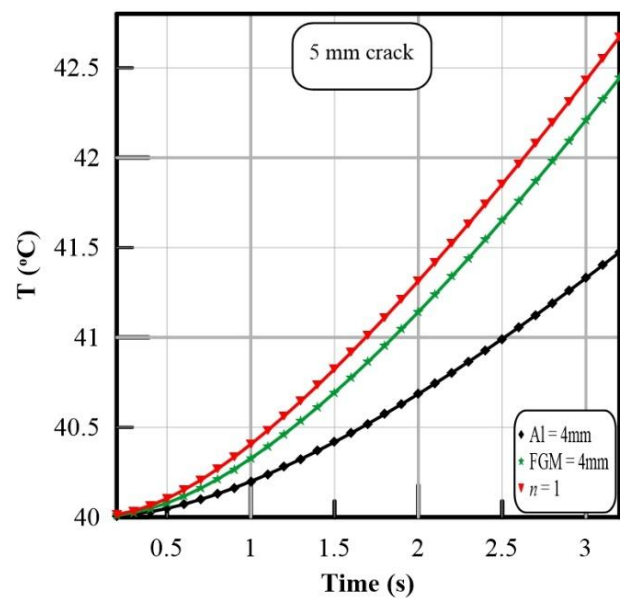
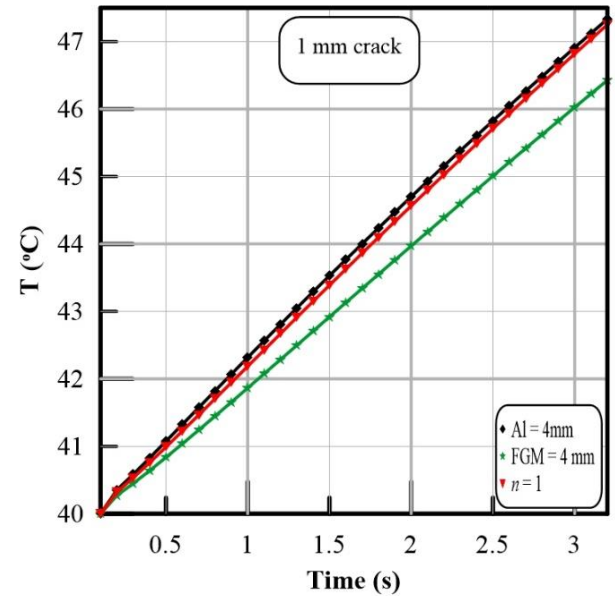


Fig. 6 Transient temperature for lined pipes

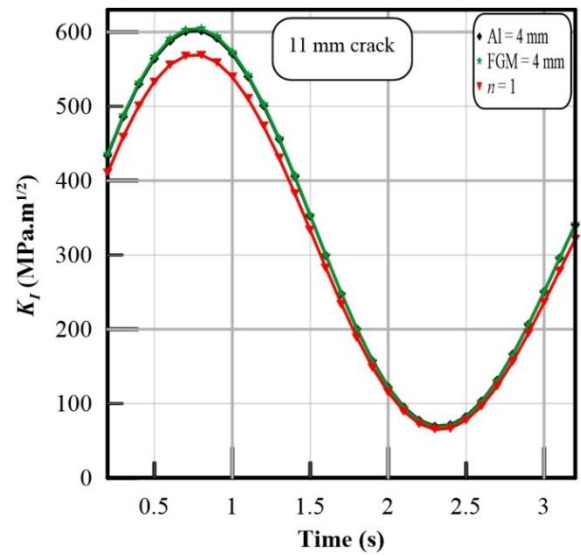
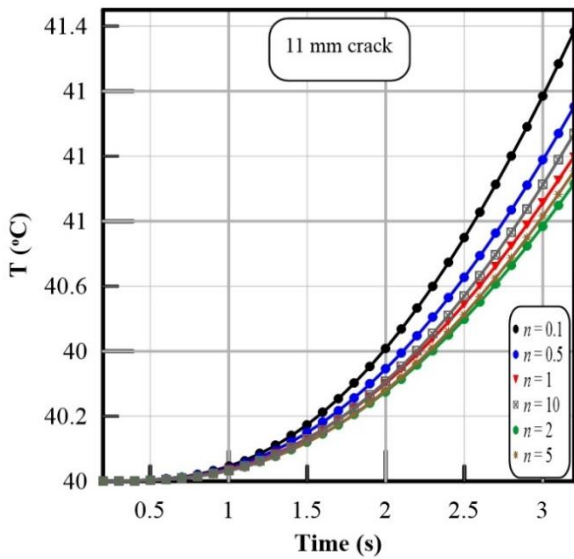
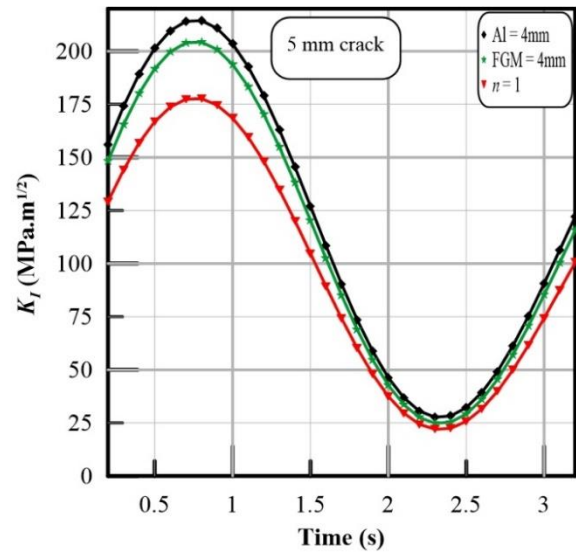
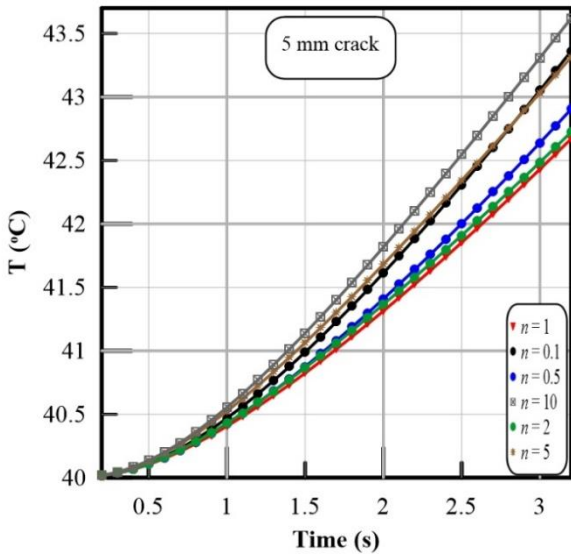
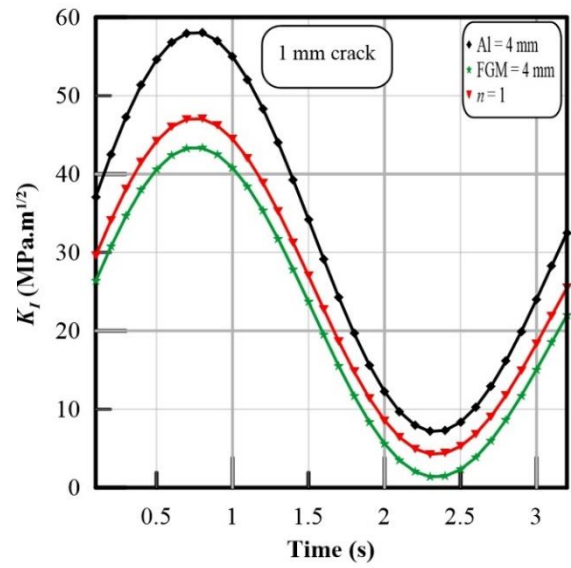
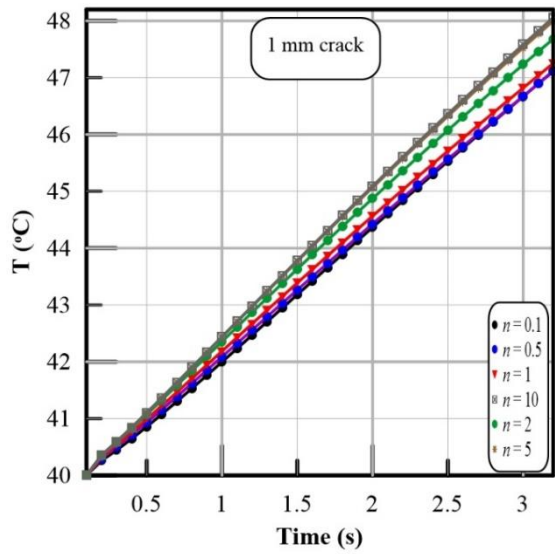


Fig. 7 Transient temperature for P-FGM pipes

Fig. 8 Stress intensity factor for lined pipes

However, at 5 mm and 11 mm, the ceramic component has more influence on the heat transferred from inside.

Stress intensity factor (K_I) at 1, 5, 11 mm cracks indicates that the second configuration (pipe lined with 4

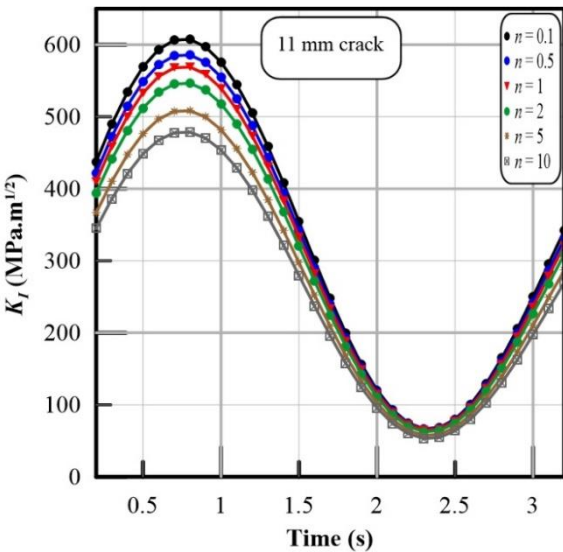
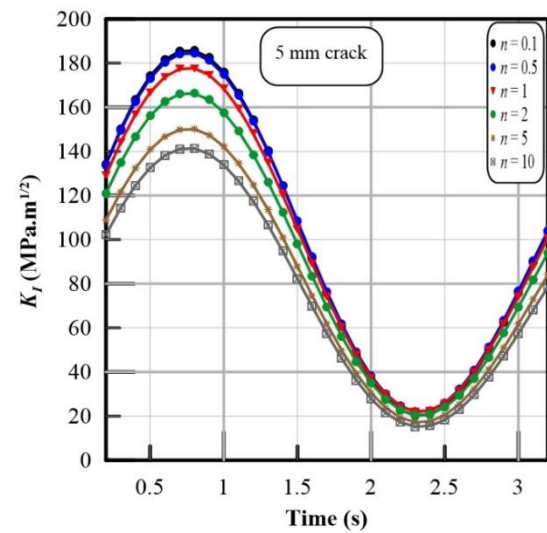
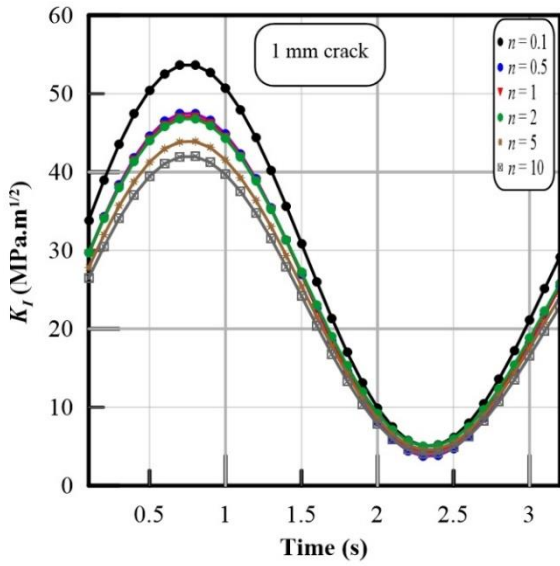


Fig. 9 Stress intensity factor for P-FGM pipes

mm Alumina from inside) presents the maximum stress intensity factor value. The first configuration (pipe lined

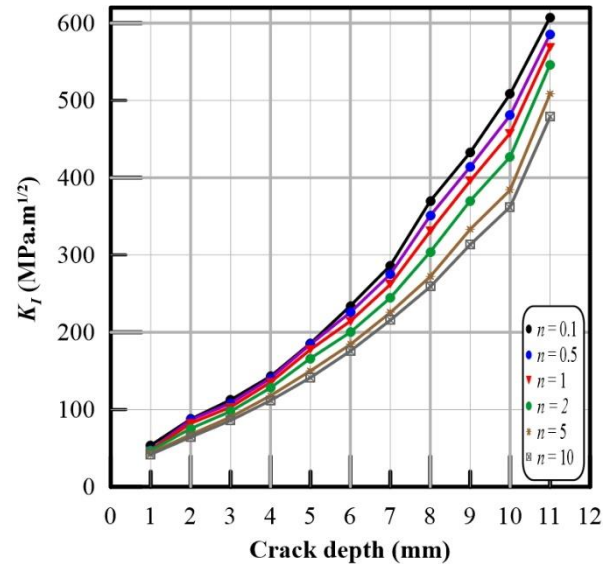
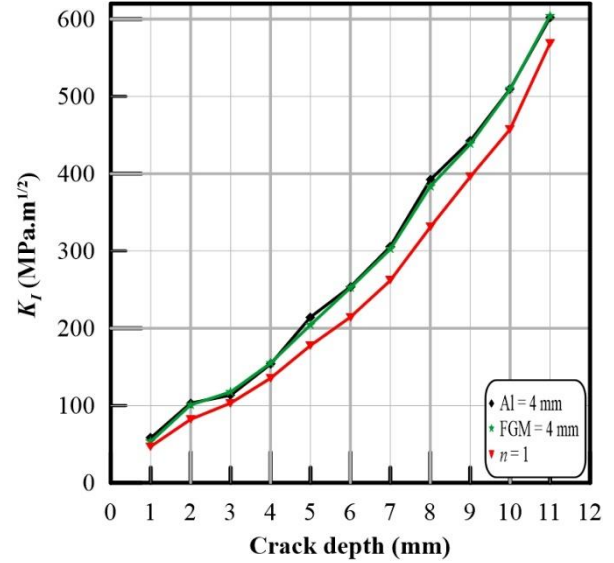


Fig. 10 The maximum Stress intensity factor

with 4 mm FGM from inside) has the minimum stress intensity factor at the shallow crack depth; however, completely FGM configuration has the minimum stress intensity factor according to the increase of the depths of crack. The stress intensity factor of the pipe lined with 4 mm Alumina converges to that of the pipe lined with 4 mm FGM by the increase of crack depth. So, the FGM pipe is more stable against crack propagation Fig. 8. The stress intensity factor is convergent for $n = 0.5, 1$ and 2 at 1 mm crack, however it is convergent at $n = 0.1$ and 0.5 at 5 mm crack. $n = 10$ has the lowest stress intensity factor at every crack depth and $n = 0.1$ has the highest stress intensity factor at each crack depth. The difference of the stress intensity factors is variable against time because of the nonlinearity of the applied load Fig. 9.

The maximum Stress intensity factor (K_I) for the three studied models against the depth of crack indicates that the pipe lined with 4 mm Alumina and the pipe lined with 4 mm FGM have converged values. The maximum Stress intensity factor of perfectly FG pipe with power factor $n = 1$

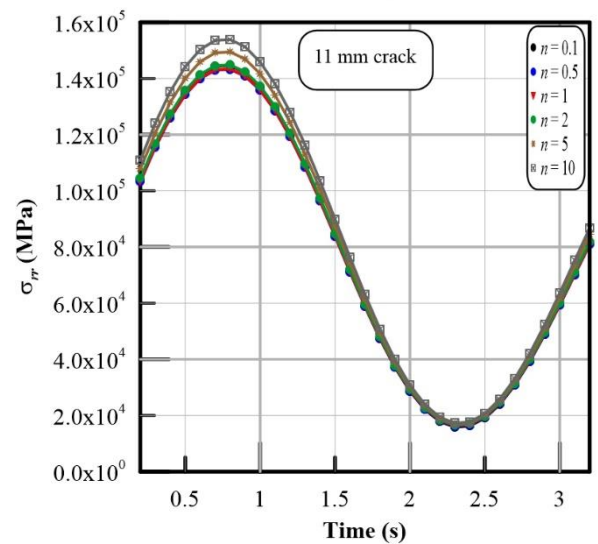
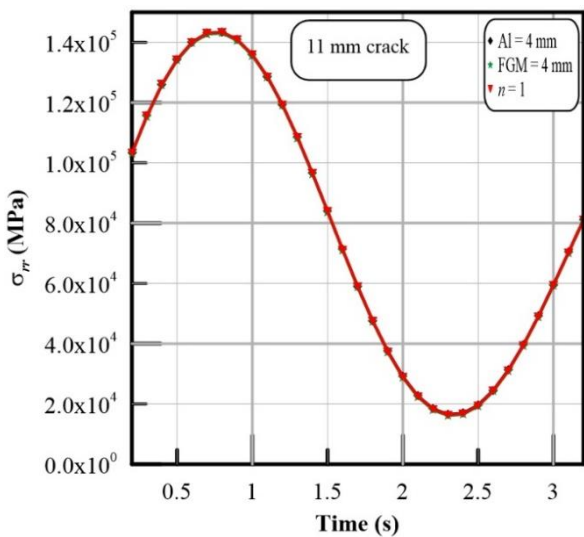
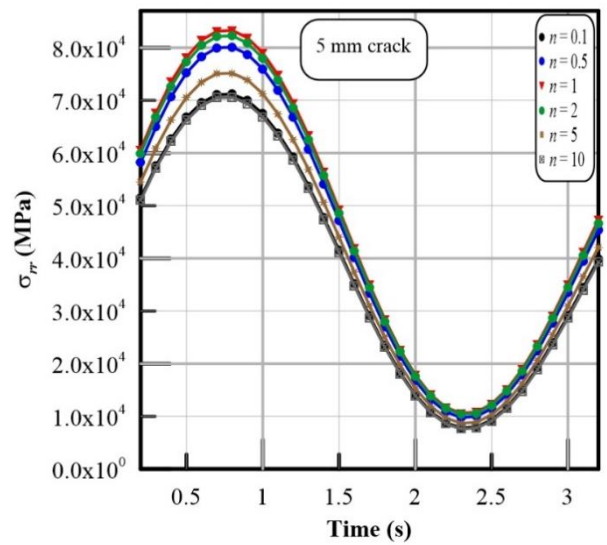
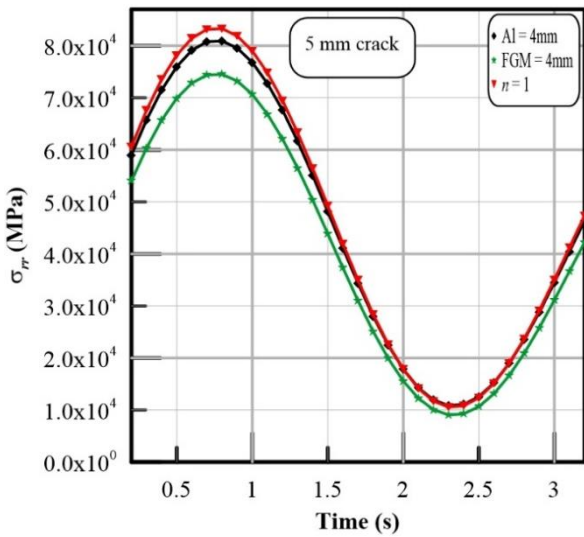
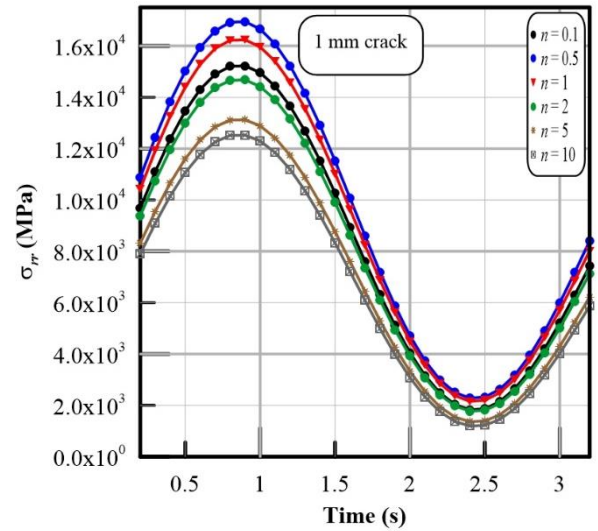
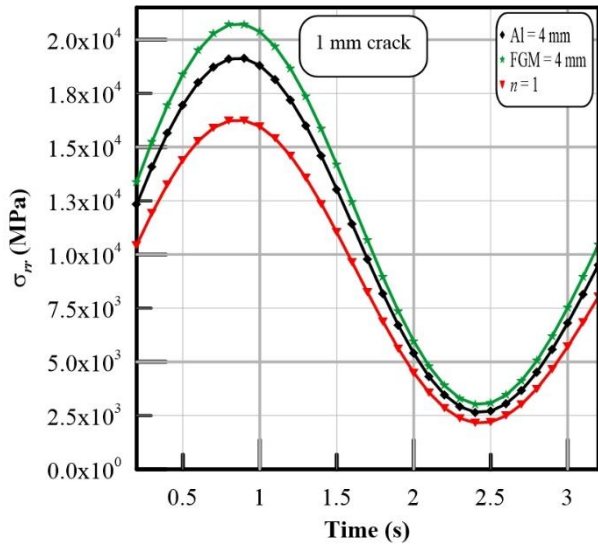


Fig. 11 The Radial Stress for lined pipes

Fig. 12 The Radial Stress for P-FGM pipes

is lower than the other pipes Fig. 10. The stress intensity factor of cracks at different depths shows that the stress intensity factor increases according to the increase of n and the depth of crack. i.e. the stress intensity factor of $n = 10$ at

8 mm crack approaches the stress intensity factor of $n = 0.1$ at 6 mm crack.

The radial stress contribution near the tip of crack is greater than its contribution in the absence of cracks and it

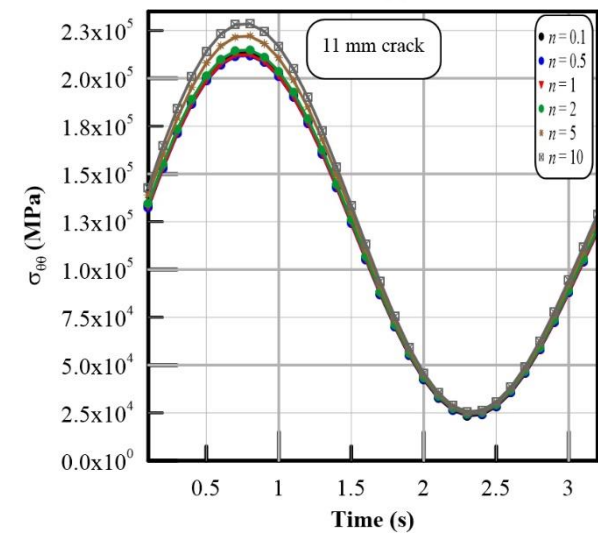
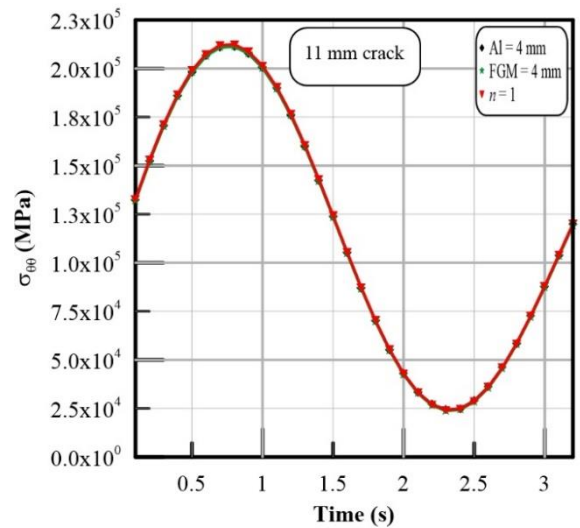
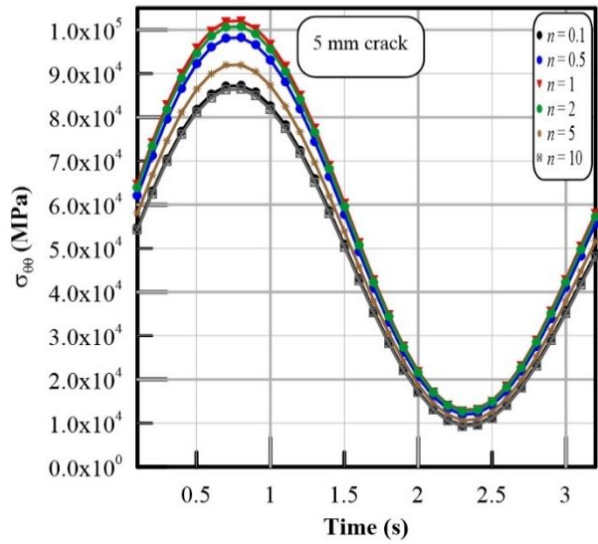
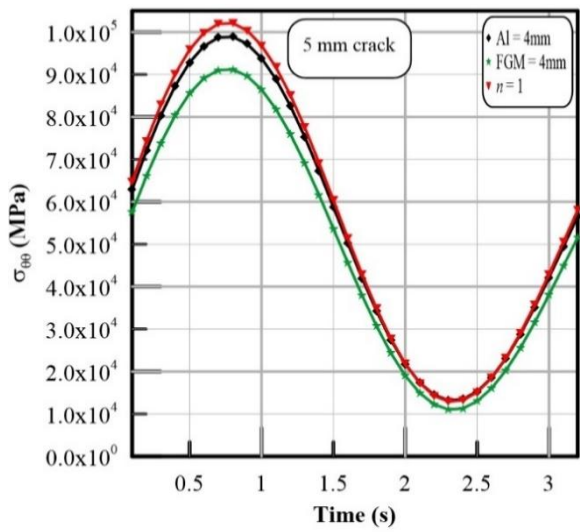
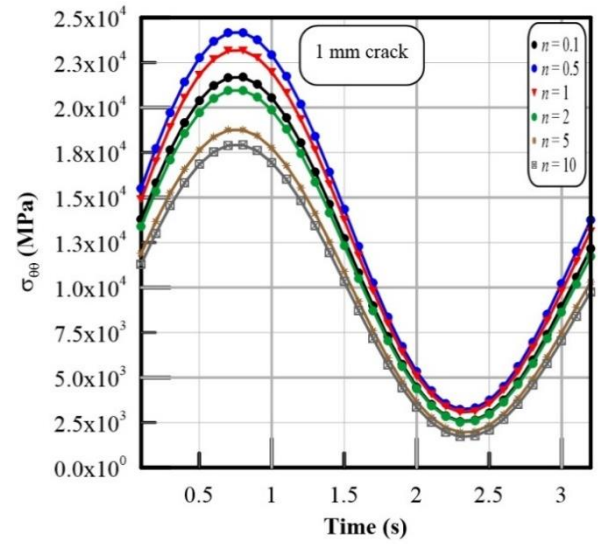
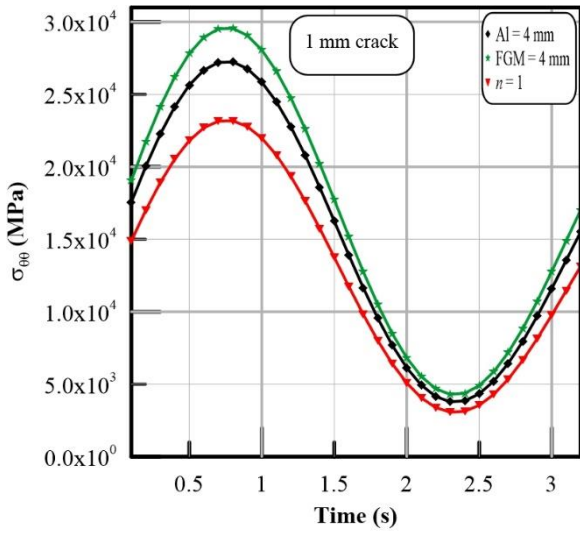


Fig. 13 The Hoop Stress for lined pipes

Fig. 14 The Hoop Stress for P-FGM pipe

has tensile stress only contrary to at the non-cracked pressurized pipes, where it mainly has compression stress. The radial stress value near the tip of crack rose extremely by the propagation of crack through the thickness. The value of the radial stress increases and converges by

increasing the depth of crack for the studied FG and lined pipes Figs. 11 and 12.

The hoop stress near the tip of the crack rises extremely by its propagation through the thickness. The hoop stress

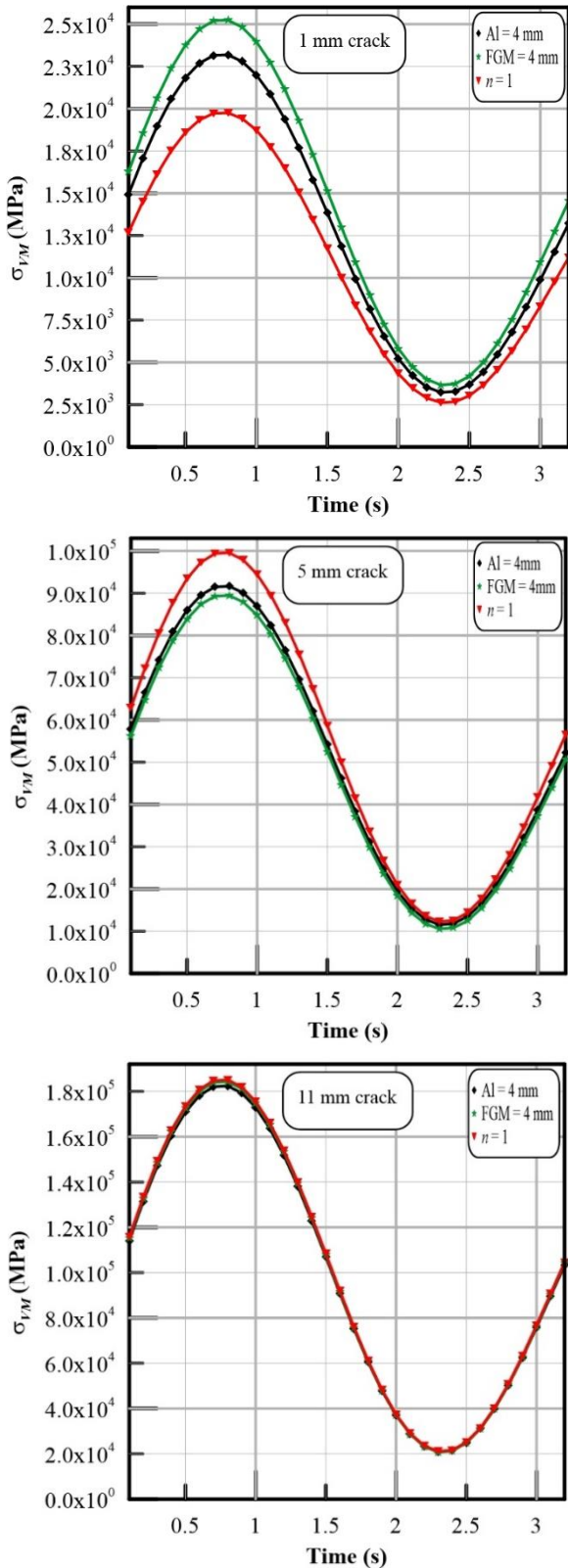


Fig. 15 The Von-Mises Stress for lined pipes

increases and converges for the different studied FGM configurations according to the depth of crack Figs. 13 and 14.

The Von-Mises stress near the tip of crack rises extremely by the propagation of the crack through the

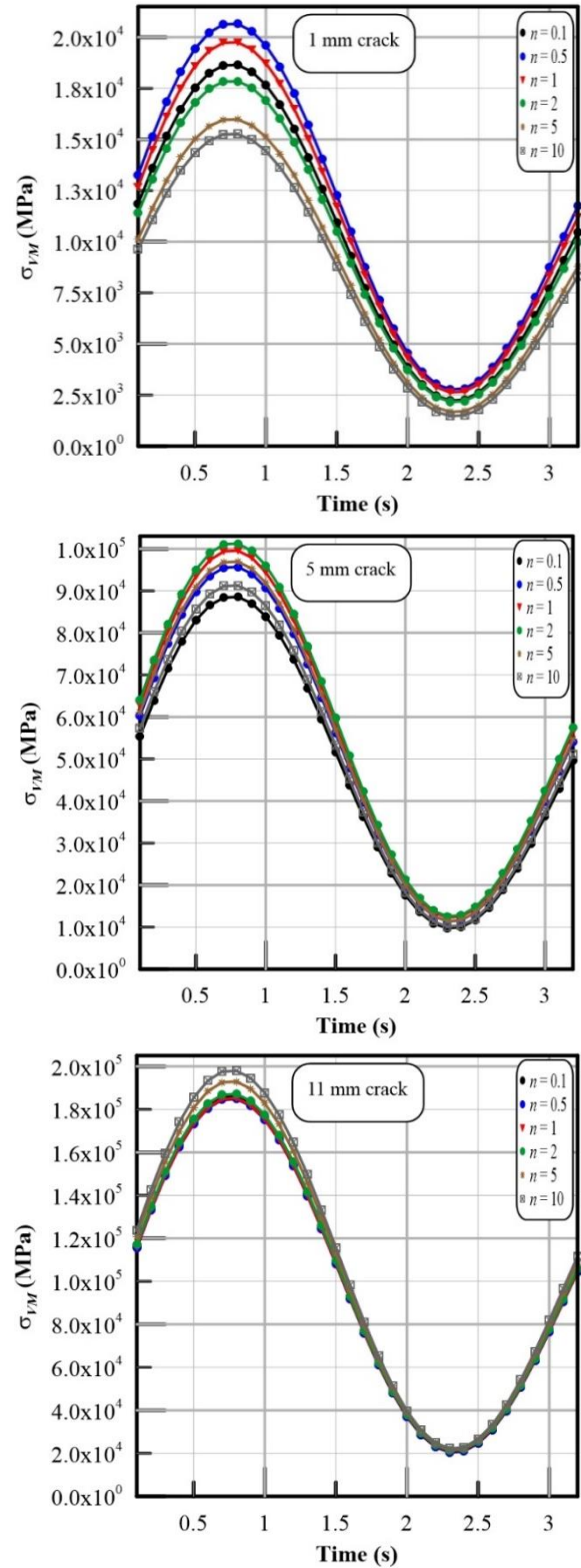


Fig. 16 The Von-Mises Stress for P-FGM pipes

thickness. The Von-Mises stress increases and converges for the different studied FGMs according to the depth of crack and the power factor as shown in Figs. 15 and 16.

The deflection varies at each crack depth with time according to the variation of material and the power factor of FGM as shown in Figs. 17 and 18.

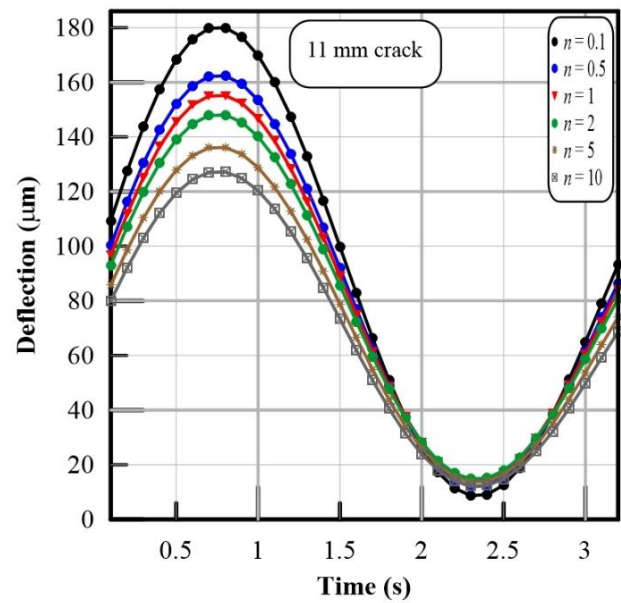
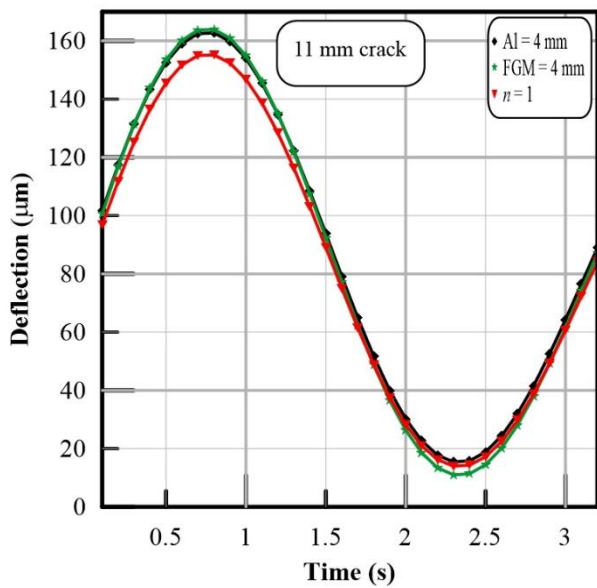
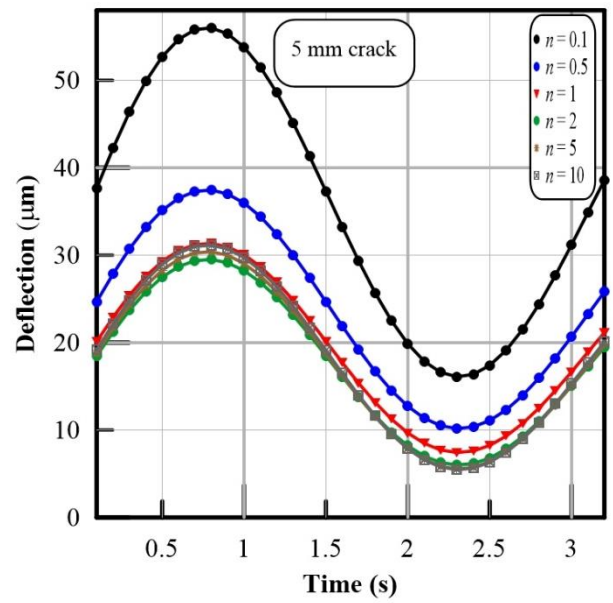
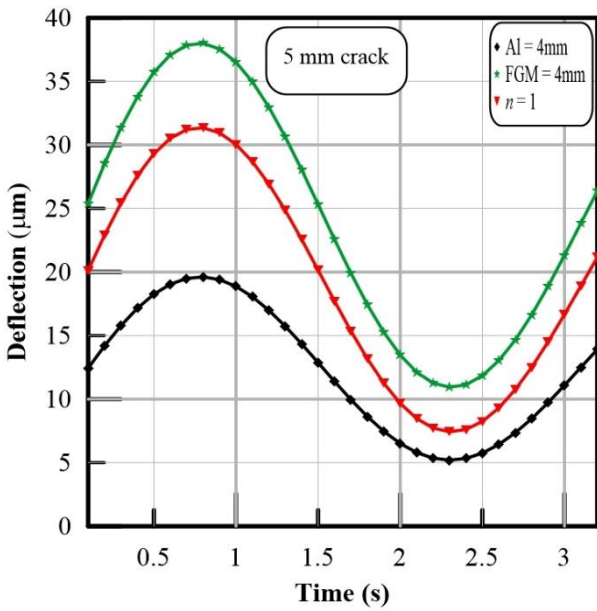
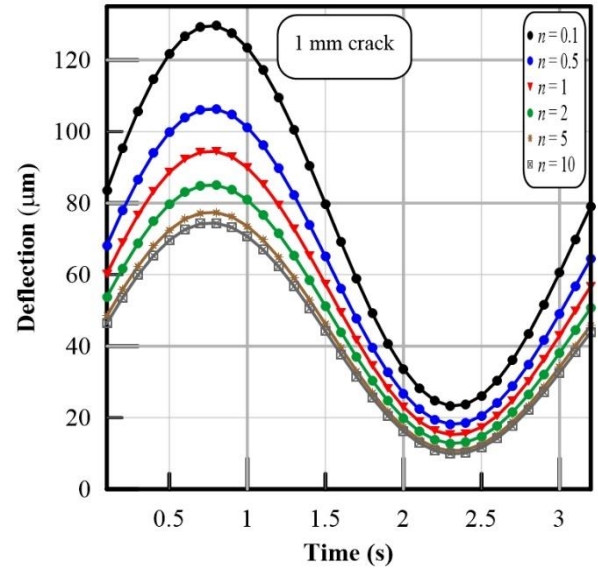
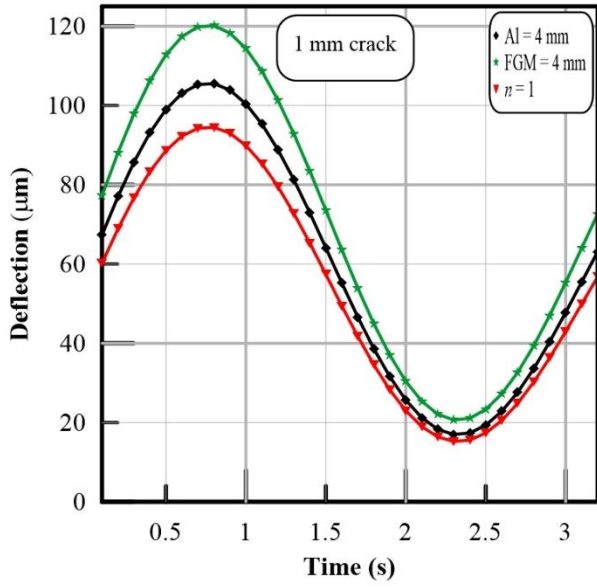


Fig. 17 The deflection at crack tip for lined pipes

Fig. 18 The deflection at crack tip for P-FGM pipes

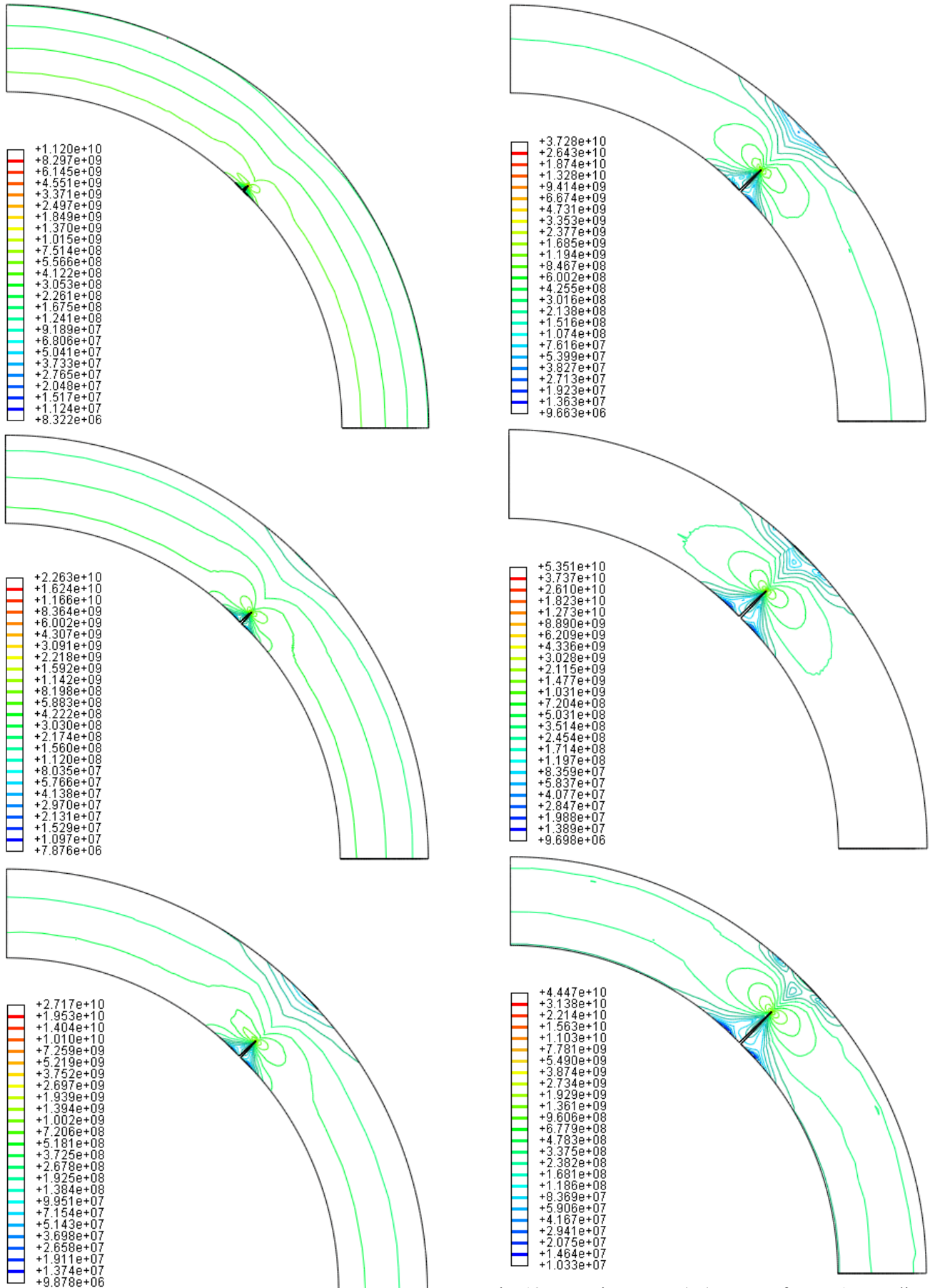


Fig. 19 Von-Mises stress (Pa) contour for $n = 1$ according to the crack depth from 1 to 11 mm at 3.2 seconds

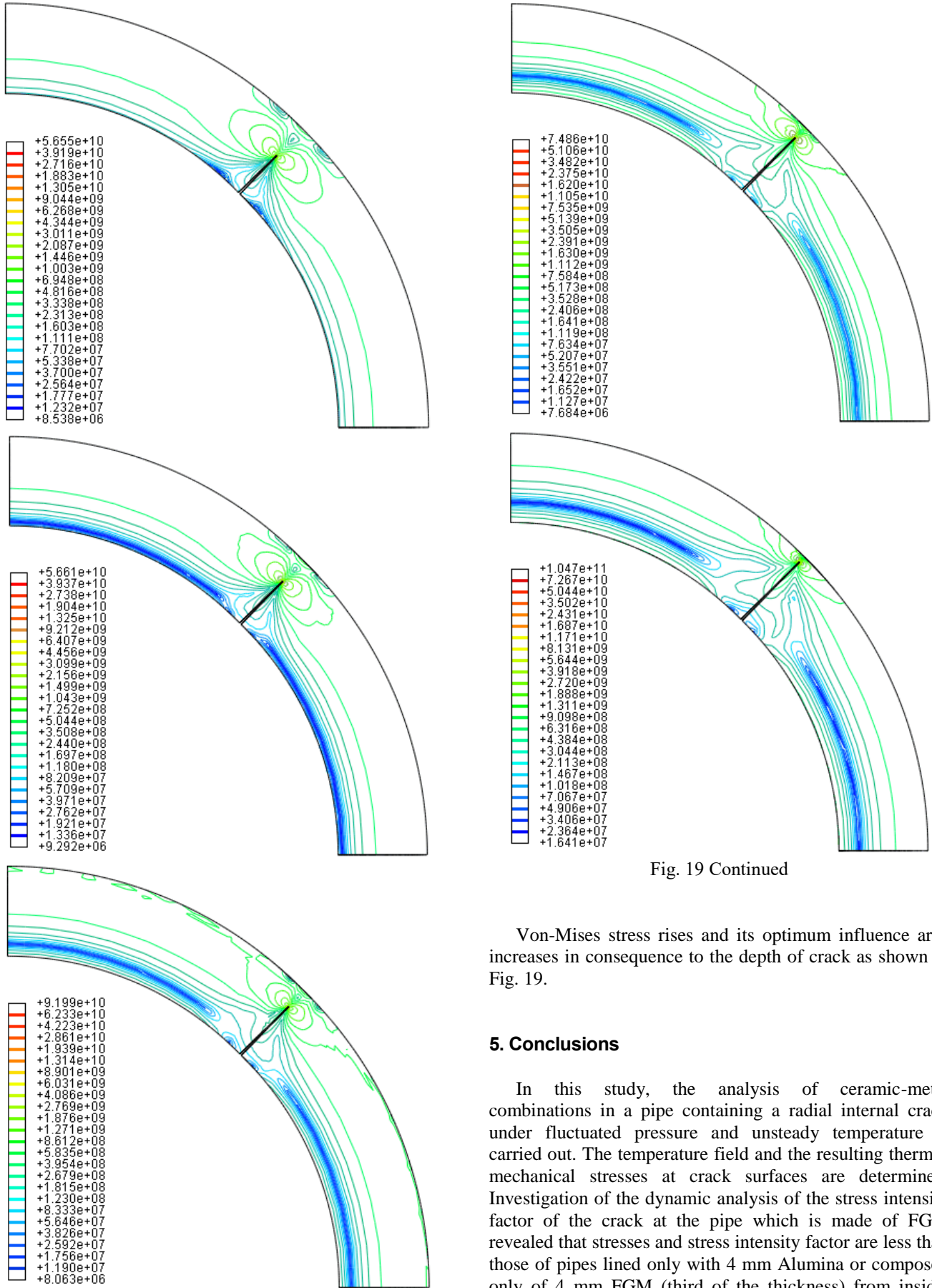


Fig. 19 Continued

Von-Mises stress rises and its optimum influence area increases in consequence to the depth of crack as shown in Fig. 19.

5. Conclusions

In this study, the analysis of ceramic-metal combinations in a pipe containing a radial internal crack under fluctuated pressure and unsteady temperature is carried out. The temperature field and the resulting thermo-mechanical stresses at crack surfaces are determined. Investigation of the dynamic analysis of the stress intensity factor of the crack at the pipe which is made of FGM revealed that stresses and stress intensity factor are less than those of pipes lined only with 4 mm Alumina or composed only of 4 mm FGM (third of the thickness) from inside. Analysis of FGM with different power indices revealed that

stresses and stress intensity factor are highly dependent on the power law index. The minimum stresses and stress intensity factors were at $n = 10$, the maximum stresses and stress intensity factors were at $n = 0.1$.

References

- Alshorbagy, A.E., Eltahir, M.A. and Mahmoud, F.F. (2011), "Free vibration characteristics of a functionally graded beam by finite element method", *Appl. Math. Model.*, **35**(1), 412-425.
- Alshorbagy, A.E., Eltahir, M.A. and Mahmoud, F.F. (2013), "Static analysis of nanobeams using nonlocal FEM", *J. Mech. Sci. Technol.*, **27**(7), 2035-2041.
- Anderson, T.L. (2005), *Fracture Mechanics: Fundamentals and Applications*, CRC Press.
- Burlayenko, V.N., Altenbach, H., Sadowski, T. and Dimitrova, S.D. (2016), "Computational simulations of thermal shock cracking by the virtual crack closure technique in a functionally graded plate", *Comput. Mater. Sci.*, **116**, 11-21.
- De Schiara, L.S. and De Ribeiro, G.O. (2016), "Finite element mesh generation for fracture mechanics in 3D coupled with ansys®: Elliptical cracks and lack of fusion in nozzle welds", *J. Brazil. Soc. Mech. Sci. Eng.*, **38**(1), 253-263.
- Eltahir, M.A., Alshorbagy, A.E. and Mahmoud, F.F. (2013a), "Vibration analysis of euler-bernoulli nanobeams by using finite element method", *Appl. Math. Model.*, **37**(7), 4787-4797.
- Eltahir, M.A., Alshorbagy, A.E. and Mahmoud, F.F. (2013b), "Determination of neutral axis position and its effect on natural frequencies of functionally graded macro/nanobeams", *Compos. Struct.*, **99**, 193-201.
- Eshraghi, I., Soltani, N. and Rajabi, M. (2016), "Transient stress intensity factors of functionally graded hollow cylinders with internal circumferential cracks", *Lat. Am. J. Sol. Struct.*, **13**(9), 1738-1762.
- Eskandari, H. (2016), "Three-dimensional investigations of stress intensity factors in a rotating thick-walled FGM cylinder", *Jord. J. Mech. Industr. Eng.*, **10**(2).
- Eskandari, H. (2016), "Stress intensity factor of semi-elliptical surface crack in a thermo-mechanically loaded cylinder with hoop wrapped FGM layer", *J. Brazil. Soc. Mech. Sci. Eng.*, **38**(8), 2563-2570.
- Francisco, J.C., Moreno, J.R., Waldek Filho, W.B. and Ruchert, C.O. (2016), "Effect of pre-crack in the fracture properties of steel pipes used in oil type API 5L X70", *J. Brazil. Soc. Mech. Sci. Eng.*, **38**(7), 2117-2127.
- Fu, J.W., Chen, Z.T., Qian, L.F. and Xu, Y.D. (2016), "Thermal fracture of cracked cylinders associated with nonclassical heat conduction: The effect of material property", *J. Therm. Stress.*, **39**(9), 1119-1137.
- Hamed, M.A., Eltahir, M.A., Sadoun, A.M. and Almitani, K.H. (2016), "Free vibration of symmetric and sigmoid functionally graded nanobeams", *Appl. Phys. A*, **122**(9), 829.
- Hein, J. and Kuna, M. (2016), "3D J-integral for functionally graded and temperature dependent thermoelastic materials", *Proc. Struct. Integr.*, **2**, 2246-2254.
- Lei, Y. (2016), "Validation of contour integral functions (J and C(t)) in ABAQUS v6.11-v6.14 for combined mechanical and residual stresses", *Proc. Struct. Integr.*, **2**, 2566-2574.
- Mirsayar, M. and Takabi, B. (2016), "Fracture of underwater notched structures", *Eng. Sol. Mech.*, **4**(2), 43-52.
- Nabil, B., Abdelkader, B., Miloud, A. and Noureddine, B. (2017), "On the mixed-mode crack propagation in FGMs plates: Comparison of different criteria", *Struct. Eng. Mech.*, **61**(3), 371-379.
- Nimje, S.V. and Panigrahi, S.K. (2016), "Effects of functionally graded adhesive on failures of socket joint of laminated FRP composite tubes", *J. Dam. Mech.*, **26**(8), 1170-1189.
- Pan, H., Song, T. and Wang, Z. (2016), "Thermal fracture model for a functionally graded material with general thermomechanical properties and collinear cracks", *J. Therm. Stress.*, **39**(7), 820-834.
- Rajabi, M. and Soltani, N. (2016), "Mixed-mode thermal fracture of AISI 304 stainless steel with temperature-dependent material properties", *Arch. Mech.*, **68**(4).
- Rizov, V. (2017), "Fracture analysis of functionally graded beams with considering material non-linearity", *Struct. Eng. Mech.*, **64**(4), 487-494.
- Shariati, M., Rokhi, M.M. and Rayegan, H. (2017), "Investigation of stress intensity factor for internal cracks in FG cylinders under static and dynamic loading", *Fratta ed Integrità Strutturale*, (39), 166.
- Sharma, K., Bhattacharya, S. and Sonkar, V. (2016), "XFEM simulation on mixed-mode fatigue crack growth of functionally graded materials", *J. Mech. Eng. Biomech.*, **1**.
- Shi, J., Chopp, D., Lua, J., Sukumar, N. and Belytschko, T. (2010), "ABAQUS implementation of extended finite element method using a level set representation for three-dimensional fatigue crack growth and life predictions", *Eng. Fract. Mech.*, **77**(14), 2840-2863.
- Sladek, J., Sladek, V., Repka, M. and Tan, C.L. (2016), "Evaluation of the T-stress for cracks in functionally graded materials by the FEM", *Theoret. Appl. Fract. Mech.*, **86**, 332-341.
- Soilam, A.E., Eltahir, M.A., Attia, M.A. and Alshorbagy, A. (2018), "Nonlinear transient analysis of FG pipe subjected to internal pressure and unsteady temperature in a natural gas facility", *Struct. Eng. Mech.*, Accepted.
- Swaminathan, K. and Sangeetha, D.M. (2017), "Thermal analysis of FGM plates-a critical review of various modeling techniques and solution methods", *Compos. Struct.*, **160**, 43-60.

CC